A Theoretical Study of the Pressure-Induced Dimerization of C_{60} Fullerene

Alexander V. Dzyabchenko*

Karpov Institute of Physical Chemistry, 10 Vorontsovo pole, 103064 Moscow, Russia

Viatcheslav Agafonov

Laboratoire de Chimie Physique, J.E. 1990, Faculté de Pharmacie de l'Université de Tours, 31 av. Monge, 37200 Tours, France

Valery A. Davydov

Institute of High-Pressure Physics, Russian Academy of Sciences, 142092 Troitsk, Moscow Region, Russia

Received: October 5, 1998

We present a theoretical study of the solid-state dimerization of C_{60} fullerene, which occurs under pressure through [2+2] cycloaddition of double bonds. The possible crystal packings of $(C_{60})_2$ molecules are calculated by minimization of the lattice energy with a bond charge intermolecular potential model proved successful in the previous C_{60} studies. The set of dimer lattices that were derived from the fcc lattice was used to construct the initial structures for minimization. The final structures found this way, although belonging to various space-group symmetries, retain approximately fcc arrangement of the constituting C_{60} cages. On the other hand, the structure obtained from the dimer motif observed in the *o*-dichlorobenzene solvate of $(C_{60})_2$ exhibits a hcp-like C_{60} arrangement. The more energetically stable hcp-type dimer seems not to form due to the high potential barrier separating the fcc and hcp structures. The relative stability of the predicted structures changes significantly under pressure. Some of the dimer structures are remarkably similar to the respective theoretical monomeric and polymeric C_{60} structures studied previously. On this basis we propose that the respective structures are connected states in the possible conversion paths from pristine C_{60} to its various polymerization products. One of the dimer structures is geometrically favorable for the formation of the higher C_{60} chain oligomers as well as of the infinite polymer.

1. Introduction

Solid C_{60} fullerene is known to polymerize through [2+2] cycloaddition of double bonds[1] under the light irradiation or pressure. Of the various pressure-polymerized C_{60} products, whose nature depends on the pressure and temperature conditions applied during product preparation, the crystalline phases of orthorhombic (O), tetragonal (T), and rhombohedral (R) symmetry are of key importance. On the basis of X-ray and spectral investigations, these phases have been unambiguously identified as polymeric crystals composed of linear chains, tetragonal layers, and hexagonal layers, respectively, where C_{60} cages are linked with each other in one or two dimensions through cyclobutane rings.[2−9] (See also ref 10 for a review paper on the high-pressure studies of fullerenes.)

The dimer is the smallest polymerized C_{60} molecule and the possibility of conversion of C_{60} monomer into the dimer is of particular interest from both theoretical and practical points of view. The $(C_{60})_2$ molecules are known to occur in films of the fcc C_{60} exposed to UV light at about 380 K.[11] The first indications on the possible dimer presence in the pressure-polymerized C_{60} were found when comparing its experimental IR and Raman spectra[12,13] with theoretical vibration spectra of free $(C_{60})_2$ molecule.[14−17] Wang et al.[18] synthesized a C_{60} dimer through solid-state mechanochemical reaction of C_{60} with potassium cyanide and then succeeded to recrystallize it in a single-crystal form (although solvated with *o*-dichlorobenzene). The subsequent X-ray structure determination has established the dumb-bell-shaped molecular structure with D_{2h} symmetry (Figure 1), indicative of the [2+2] cycloaddition product.

An alternative structure conforming to C_i symmetry, with a single-bonded trans junction between the two buckyballs, was established for the $(C_{60})_2$ dianion by Oszlányi et al.[19] as a result of an X-ray powder diffraction study of the crystalline product $K_2(C_{60})_2$, which was prepared by the solid-state reaction of metallic K with powdered C_{60}.

The availability of the IR[20] and Raman[21] spectra of the D_{2h} dimer have made it possible to finally identify this dimer as one of the products of C_{60} polymerization characteristic of a low-pressure region.[22] At the same time, the crystal structure of the proposed dimer phase remained unknown, for the dimer was contaminated with both the starting monomer and 1D and 2D polymeric products. Its X-ray diffraction pattern showed no significant changes in comparison to the fcc C_{60}, except that all lines of this pattern were broadened and shifted to higher angles. This was interpreted in terms of crystal disorder resulting from the displacements of C_{60} cages from their exact fcc position toward each other in the directions of their closest contact along cubic face diagonals.[22]

The establishment of crystal structure of the pressure-induced C_{60} dimer would be of particular interest in view of the currently discussed solid-state conversion mechanisms of the monomer into its various polymerization products, where the dimer phase can be proposed as an intermediate. To get more of an idea on its possible structures, we performed a computational search

10.1021/jp983951w CCC: $18.00
Published on Web 03/26/1999

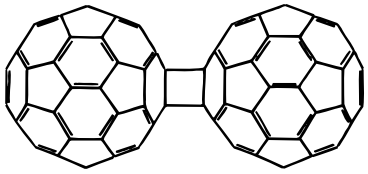

Figure 1. Molecular structure of $(C_{60})_2$.

for its optimal crystal packings, where $(C_{60})_2$ molecules were treated as rigid bodies of known shape and dimensions. Some preliminary results of this theoretical study have been reported before.[22]

The plan of the paper is as follows. Section 2 summarizes the previous theoretical work on the structure prediction of monomeric C_{60} and its pressure-polymerized products. Section 3 presents a qualitative model of the disordered dimer structure formation consistent with the observed X-ray diffraction pattern. Sections 4 and 5 contain the computational details and a brief description of the PMC program used throughout this work for crystal packing calculations. Section 6 describes the main results of the computations. They involve the consideration of the *o*-dichlorobenzene solvated dimer[18] and of the K-doped trans-dimer[19] in an attempt to predict their experimentally observed structures and thus provide additional tests for the interaction potential model. Then the search for the pure dimer packings connected to the fcc C_{60} is described, including characterization of the final minima and their behavior under pressure. In Section 7, the similarities between the most stable dimer packings and the previously found theoretical monomeric and polymeric C_{60} packings are discussed in connection with the possible conversion mechanisms from monomeric to polymerized C_{60}.

2. Previous Theoretical Work

The problem of key significance in most previous theoretical studies of solid fullerene and fullerene-based materials concerns the correct prediction of crystal structure and physical properties of C_{60}. The very first attempt[23] to predict the crystal structure of C_{60} at 0 K using atom−atom potentials of purely Lennard-Jones (LJ) type resulted in an orthorhombic structure, which was not confirmed by experimental evidence for the low-temperature form. The latter is in fact simple cubic, of *Pa*3 space group, with molecules occurring in two orientational states, one of which in the more energetically stable pentagon-oriented (P) state (pentagon of one molecule faces the double bond of another) and the less stable hexagon-oriented (H) state (hexagon faces double bond).[24] In the subsequent studies[25−31] it was well recognized that the simple atom-centered LJ interactions do not account correctly for the orientational ordering in pure C_{60} and a number of electrostatic point charge interaction potential models[25−28] have been suggested. Three of them[25−27] were identical with respect to the location of the negative electrostatic charges $-2q$ at the middles of the 30 C−C double bonds but differ in distribution of the total positive charge ($60q$) over the molecule. Thus Lu et al.[25] place positive charges q at the centers of the 60 single bonds, Sprik et al.[26] assigned the same charge to each carbon atom, while Burgos et al.[27] positioned the charges $5q$ at the twelve pentagonal centers. Pintschovius and Chaplot[28] introduced a split-bond charge model: where the charge q is at the carbon atom and where the double bond charge of $-2q$ is split in the radial direction in two charges ($-q$), inward and outward, of the surface of the molecule.

Using the potential model of Lu et al.[25] we performed a global search for the energy minima of C_{60}, which involved a few space groups most common in organic crystals.[29] The global and local minima found with one model were then used[30] as initial ones to obtain the corresponding lists of minima with the other bond charge models.[25−28] A comparison of these results has shown that all models provide in the global minimum a structure that agrees fairly well with respect to the space-group symmetry, lattice dimensions and molecular orientation with the observed P state of the low-temperature form. However, with respect to the H state, two models[26,27] were found not good. Thus, the model of Burgos et al.[27] predicts the molecule orientated by 30° away from that in the H state.[24] In addition, this model provides a minimum of monoclinic symmetry lower in energy than that of the H state. As to the model of Sprik et al.,[26] we found that it does not show any presence of the H-state minimum (unless the minimized structure was constrained by *Pa*3 symmetry). In contrast, the model of Lu et al. provides the H structure in reasonable agreement with the experimental one and the correct stability ranking for the whole structure list, where P is more stable than H and both are more stable than the hypothetical structures (Table 1) found by the global search.[30] Finally, as we found quite recently,[31] the split-bond charge model of Pintschovius and Chaplot[28] results in the minima which are remarkably similar to all those obtained with the Lu et al. model with respect to both the geometry and the energetic stability.

The model of Lu et al. has also proved to be successful in the prediction of the pressure dependence of the observed C_{60} structures.[32,33] Thus, it predicts the P/H transition point at a pressure of about 6 kbar,[32] close to the critical point in the anomalous region of the bulk modulus vs pressure dependence measured experimentally.[34] At a higher pressure (∼40 kbar) it predicts one more transition: from *Pa*3-H to a hypothetical orthorhombic phase of *Cmca* symmetry that is of highest density.[33] It is interesting to note that this structure does not occur as an energy minimum without pressure, being a stationary point instead, but can be found as the global minimum if calculated with the purely LJ potential.[29,30]

The energy minimization was applied further then to predict the crystal packing in the polymerized C_{60} phases, assuming fixed internal geometry for polymeric chains and layers.[8,9,35−38] This resulted in new structures for the three polymeric phases (Table 2) which were more energetically preferable than those reported by Núnez et al.[3]

Thus with the O phase, the optimized chain orientation ($\psi = 61°$) results in the *Pnnm* space group[8,35−37] rather than *Immm* ($\psi = 0°$ or 90°) suggested by Núnez et al.[3] The *Pnnm* symmetry was also reported by Moret et al.[7] who studied single-crystal specimens of the O phase by X-ray diffraction. Unfortunately, this experiment was unable to identify the rotation angle: the data could be equally well described by both a 45° angle (identical to that found in the polymerized alkali metal fulleride) and the theoretically predicted 61° angle.

In addition to the *Immm* structure of the T phase, which assumes the stacking of tetragonal layers on one another through volume-centering translation,[3] we suggested a more energetically stable structure of $P4_2/mmc$ symmetry, where successive layers are related through 4_2 screw axis.

Concerning the R phase, we found that a new rhombohedral structure ($R\bar{3}m$-II), more stable than previously known[3] is obtained if the latter structure ($R\bar{3}m$-I) is modified by rotating the C_{60} cage through 60° about the $\bar{3}$ axis. (This can be equally described as a reversal of the sequence of the layers in their infinite stack along c).[37] One more $R\bar{3}m$ structure (III), with six C_{60} per unit cell, is of still lower energy than the former two. It comprises both C_{60} orientations that occur in successive

TABLE 1: Predicted Structures of Monomeric C_{60} Fullerene[a]

structure	exptl P/H[b]	*Pa*3-P	*Pa*3-H	$P2_1/n$	*Cmca*	$\sim P4_2/m$[c]	$R\bar{3}$
E_{tot} (kcal/mol)		−44.08	−43.45	−42.91	−42.48	−42.47	−42.71
E_{Coul}(kcal/mol)		−4.20	−1.76	−3.22	0.22	−2.30	−2.70
density (g/cm^3)	1.728	1.79	1.81	1.78	1.82	1.79	1.79
cell dimensions (Å, deg)							
a	14.045	13.88	13.83	13.80	13.98	9.85	9.91
b	14.045	13.88	13.83	9.92	9.71	9.84	9.91
c	14.045	13.88	13.83	9.80	9.71	13.81	23.62
α	90	90	90	90	92.6	90.3	90
β	90	90	90	91.3	90	89.8	90
γ	90	90	90	90	90	90.6	120
Euler angles (deg)							
ϕ	−14.2/18.4	−14	15	21	−11	7; −8	0
θ	−11.1/25.2	−11	19	−7	−7	1; 3	0
ψ	−14.2/18.4	−14	15	−72	−69	13; 105	45
r[d] (Å)	3.87/3.61	3.77	3.71	3.46	3.36	3.45−3.73	3.60
λ[e] (deg)	35.6/17.0	34	11	0	0	0	0
ω[f] (deg)				23	14	17; 14	15

[a] From ref 30. [b] Reference 24. [c] Two independent molecules. [d] Center-to-center distance between the double bonds forming the closest intermolecular contact. [e] Angle between the vectors of two double bonds forming the closest intermolecular contact. [f] Turn angle relating C_{60} orientation in the monomer structure with that in the respective polymeric structure (see last paragraph of section 2).

TABLE 2: Predicted Crystal Structures of Polymeric C_{60} Products[a]

polymer	linear chain	tetragonal layer		hexagonal layer			
structure	*Pnnm*	*Immm*	$P4_2/mmc$	$R\bar{3}m$-I	$R\bar{3}m$-II	$R\bar{3}m$-III	$P6_3mc$
E_{tot} (kcal/mol)	−42.9	−37.2	−38.4	−44.5	−49.4	−51.1	−51.1
E_{Coul} (kcal/mol)	−1.5	1.42	0.2	3.5	0.8	−2.2	−2.2
density (g/cm^3)	1.89	1.96	1.96	1.96	2.02	2.01	2.01
cell dimensions (Å, deg)							
a	14.38	9.09	9.09	9.17	9.17	9.17	9.17
b	9.69	9.09	9.09	9.17	9.17	9.17	9.17
c	9.10	14.78	14.74	25.11	24.34	49.01	16.35
γ	90	90	90	120	120	120	120
ψ (deg)	61	0	0	0	60	0; 60	0; 60

[a] From refs 37 and 38.

layers in an alternate way. The two-layer packing with alternate orientations resulting in hexagonal $P6_3mc$ symmetry is of the same packing energy as the six-layer one (Table 2). Evidently, one can design more layer sequences on the basis of the given ones. From this note it follows that a kind of *orientational polytypism* is possible in the packing of layers, resulting in the disorder of C_{60} in the observed diffraction patterns.

A remarkable feature of some of the hypothetical C_{60} structures is that they, in contrast to the *Pa*3-P and -H structures, provide close intermolecular contacts with perfectly parallel arrangement of double bonds suitable for [2+2] cycloaddition (these are characterized by parameters r and λ in Table 1). Moreover, there exists a similarity of the monomeric with the respective polymeric structures, which can be seen from a comparison of their lattice dimensions and C_{60} rigid-body parameters listed in Tables 1 and 2. Thus, the *Cmca* and $P2_1/n$ structures of the monomer are similar to the *Pnnm* structure of the chain polymer. Likewise, the quasi-tetragonal $\sim P4_2/m$ structure of the monomer is similar to the $P4_2/mmc$ structure of the tetragonal-layer polymer, and the $R\bar{3}$ structure of the monomer is similar to the $R\bar{3}m$-II structure of the hexagonal-layer polymer.[38]

3. Model of Crystal Disorder

The experimentally observed X-ray diffraction pattern of the pressure-dimerized C_{60} is compatible with that of the fcc C_{60} phase except that all lines are broadened and shifted to the greater angles.[22] This is interpreted in terms of a disordered fcc C_{60} lattice, where each C_{60} shifts from exact fcc position in the direction of one of its twelve nearest neighbors to form a dimer molecule. The magnitude of this shift $s = (d_1 - d_2)/2$, where d_1 is the distance between the nearest-neighboring molecules in the fcc C_{60} and d_2 is the same distance within the dimer molecule. With $d_1 = 10$ Å and $d_2 = 9.1$ Å (according to the coordinates of the dimer molecule found by Wang et al.),[18] we have $s \sim 0.5$ Å.

The general picture of the disordered dimer formation from the fcc C_{60} is as follows. At normal pressure, the dimer state is thermodynamically less stable than the monomeric one and therefore the dimers do not form. When pressure is applied, the dimer gains in stability over the monomer because of its smaller volume. Under thermal agitation, the C_{60} molecules oscillate in the three dimensions about their fcc positions. If the thermal energy is high enough to overcome the potential barrier of [2+2] cycloaddition, the dimers form along ⟨110⟩. The dimer lifetime is finite, depending on the particular pressure and temperature conditions. The system behavior can be described as the motion of buckyballs between the locally stable positions corresponding to various dimer solid configurations. In this state, the thermodynamic equilibrium is maintained due to a "switching mechanism", in which new interfullerene bonds are formed while breaking old ones.

On cooling to lower temperatures, the predominant motion changes to the translations and rotations of dimeric molecules as a whole, which requires less activation energy than the switching mechanism. At room temperature, the disordered solid system cannot relax to an ordered crystal for kinetic reasons. Consequently, the system comes to a domain structure, with crystalline order within a domain and disordered packing of domains itself. As our calculations show (see subsequent section), the most energetically favorable structures belong to various low-symmetry groups, at the same time retaining the approximately fcc lattice geometry for C_{60} positions. The domains itself occur in the various orientations connected to cubic symmetry of the monomer. Because the internal structure of a domain itself still is not perfectly fcc, a certain incompatibility of the adjacent lattices in the interdomain region is present, which results in the variation of domain orientations. This can explain the line broadening in the experimental X-ray diffraction pattern.

It is interesting to note that, according to the Woodward−Hoffmann (WH) rules, the thermally activated [2+2] cycloaddition of two ethylene groups constitutes a difficult process due to the high activation barrier. The pressure-induced cycloaddition of solid C_{60} thus presents a remarkable exception of these rules, which can be explained by the following arguments. First, the molecular and electronic structure of pure C_{60} preclude formation of products other than of the cycloaddition type. Thus, a single-bonded trans-dimerized C_{60} product, which could be suggested as an alternative to the [2+2] product, is a biradical unstable in the absence of an electron donor agent such as the alkali metal in $K_2(C_{60})_2$.[19] The second factor is pressure that promotes the reaction by lowering its potential barrier toward the product of smaller volume.[39] The third factor, which is of prime interest to us in this paper, is a particular crystal packing that holds the double-bond fragments close together in favorable orientation with respect to one another, thus increasing the "effective section" of the [2+2] cycloaddition reaction.

4. Crystal Packing Calculations

The crystal lattice energy calculated with an empirical intermolecular potential was minimized with respect to the lattice constants and rigid-body parameters of the dimer molecule. The $(C_{60})_2$ molecular structure was assumed to be of D_{2h} symmetry and composed of two undistorted C_{60} cages of I_h symmetry, with C−C distances of 1.39 and 1.45 Å for double and single bonds, respectively. The interfullerene distance was set to 9.091 Å observed in the solvated dimer structure.[18] (This results in the cyclobutane ring dimensions of 1.39 by 2.151 Å.) We thus ignore distortions of the C_{60} cage geometry in the region of the [2+2] interfullerene linkage, assuming that the atoms involved in this link are screened out by the bulky C_{60} cages and their influence on the crystal packing is minimal. In the reference orientation, the dimer molecule was aligned with the 2-fold axes of the fullerene cages parallel to the Cartesian axes, with the longest axis of the dimer (N), corresponding to ψ rotation, directed along **Z** (see section 5).

The interaction potential for the $(C_{60})_2$ molecule was assumed identical to that used in our previous work on C_{60} structures and principally the same as proposed by Lu et al.[25] In particular, the C···C van der Waals interactions were described by the LJ type potential of the form $V(r) = \epsilon[2(\rho/r)^6 - (\rho/r)^{12}]$, with the minimum ϵ of −0.0722 kcal/mol at the equilibrium distance ρ = 3.7 Å. The Coulomb forces were modeled by effective charges of −0.5 and +0.25 electron at the centers of double and single C−C bonds, respectively.

The packing optimizations were carried out using the PMC program (see section 5). Another tool intensively used throughout the present work is the program CRYCOM for crystal-structure comparison.[40] The use of this program in the analysis of packing search results for C_{60} has been described in ref 41.

5. Program PMC

The PMC program (Packing of Molecules in Crystals)[42,43] serves for calculation of optimal packing of organic molecules by minimization of the lattice energy with respect to the six lattice constants and the 6*N* rigid-body molecular parameters of *N* independent molecules constituting the crystal structure. Of the six molecular parameters, three are center-of-gravity coordinates, *u*, *v*, *w*, of the molecule, expressed as fractions of the unit-cell edges. The other three are Euler angles, φ, θ, ψ, defining the rotation of the molecule about three *different* local axes, **L**, **M**, and **N**. The latter are normally taken mutually orthogonal and aligned with the molecular-symmetry elements. With the orthogonal **LMN** system, the effect of φ,θ,ψ-rotation on orthogonal atomic coordinates **x** is expressed by $\mathbf{x}' = R\mathbf{x}$, where

$$R(\varphi,\theta,\psi) = \begin{bmatrix} \cos\psi\cos\theta & -\sin\psi\cos\theta & \sin\theta \\ \cos\psi\sin\theta\sin\varphi + \sin\psi\cos\varphi & \cos\psi\cos\varphi - \sin\psi\sin\theta\sin\varphi & -\cos\theta\sin\varphi \\ -\cos\psi\sin\theta\cos\varphi + \sin\psi\sin\varphi & \cos\psi\sin\varphi + \sin\psi\sin\theta\cos\varphi & \cos\theta\cos\varphi \end{bmatrix}$$

The Cartesian system OXYZ is attached to the crystal axes **a**, **b**, **c**, in such a way that the unit vectors **Z** and **Y** are directed along **c** and **b***, respectively, while **X** is the vector product of **Y** and **Z**.

The energy is calculated with pairwise interatomic functions (atom−atom potentials) comprising the Ar^{-6} and Br^{-12} (or $Be^{-\alpha r}$) terms, to account for the van der Waals attractive and repulsive energies, respectively, and the $qq'r^{-1}$ term, to account for the Coulomb energy of partial charges *q* associated with atoms or special charge centers, as in the case of bond charge models for C_{60}.

To speed up lattice energy calculation, we use after Williams[44] the convergence acceleration method (an Evald-like summation of the energetic terms) for r^{-6} and r^{-1}, in which the reciprocal-lattice sum is neglected at an appropriate choice of the convergence constant *K* and the cutoff r_{cut}. We improved this method, however, by avoiding the necessity of the geometric-mean combination rule $(A_{\alpha\beta})^2 = A_{\alpha\alpha}A_{\beta\beta}$ imposed by Williams' procedure on the potential-field parameters at the attraction term (α and β designate atomic types).[42]

Another modification concerns the calculation of Coulomb energy at the end minimization point, where we add the reciprocal-lattice sum E^*_{Coul} to the minimized lattice energy E_{min} (calculated with no such correction), giving the total lattice energy E_{tot} used for comparison with other minima.[30]

When summing the lattice energy, we take into account the contact identity that occurs in the contacts of the central molecule with image molecules generated by the space-group operators. A simple theorem states that any image molecule M_i, generated by operator $(F_i, \mathbf{t}_i)$ from the central molecule M_o, possesses the same geometrical contacts with M_o as M_o with an image $M_{i'}$ generated by $(F_i^{-1}, -F_i^{-1}\mathbf{t}_i)$. We use this property, together with the crystallographic site symmetry of the molecule, to select a unique set of intermolecular contacts with corresponding multiplicity factors that enter into the expressions for the lattice energy and its analytical first derivatives.[42]

For local search we use VA09A,[45] a quasi-Newton optimization procedure operating with analytical first derivatives. Specifically in the crystal case, however, there is a problem that the finite cutoff r_{cut} makes the minimized energy function in fact discontinuous. Gibson and Scheraga[46] use cubic splines to smooth interatomic potential functions to zero at $r = r_{cut}$ and thus avoid discontinuity. We provide another way to solve this problem, which consists of the use of a *fixed list* of interatomic contacts contributing to the minimized energy function. This list is prepared according to the $r < r_{cut}$ criterion at the start of the minimization and then held unchanged until the minimum of an approximate energy function is reached. At this point the list is updated and the minimization is continued as above to give the next approximation. The whole procedure is continued repeatedly until the convergence in both the minimized energy and optimal structural parameters after two successive list updates is reached.[43] Intermediate list updates, however, are possible in the course of minimization in the event of the current structural changes after the last list update has exceeded in magnitude some user-specified limits.

The cutoff 9 Å and the convergence constant $K = 0.175$ Å^{-1} are normally used in our calculations to find local minima accurately enough at a reasonable computational effort. Our tests show that, for optimizations started from completely different structures, the program provides identity for the final structures (in case they came to the same or symmetry minima) within 0.01 kcal/mol in the lattice energy, 0.001 in translational and 0.1° in rotational parameters, 0.01 Å in the cell axis lengths, and 0.1° in the cell angles.

Our method of global investigation of the lattice-energy function[47−50] involves consideration of its symmetry in the multidimensional parameter space.[47] This gives the fundamental (asymmetric) region of the structure-parameter space that is scanned over by the grid search procedure. We use the empirical data of Belsky and Zorkii[51] on the abundance of the organic crystal structural classes (the structural class of a given structure is characterized by its space group and the positional symmetry of the molecule) as a guide to select for the global search the most likely ones that are compatible with the free-molecule symmetry.[50] The structures found by minimization under symmetry constraints are then checked to discriminate actual minima from saddle points by unconstrained minimization, where all molecules within a triclinic cell (or a supercell) are allowed to move independently of each other. At the final step of a global search we use the program CRYCOM[40] for the analysis of search results. This involves the identification of nonunique minima and determination of space-group symmetry for particular structures.[41]

Examples illustrating the PMC use with various organic molecules can be found elesewhere.[48−53] They include the first attempted prediction of the benzene structures by global energy minimization.[48a] The hypothetical structures found by us were used by others for the comparison with their own results for benzene.[54−56] The most recent investigation of this problem by van Eijck et al.[56] is the most complete with respect to the space groups covered and provides the most number of hypothetical structures. We have tested the new structures of van Eijck et al.[56] with PMC and obtained full identity, except for some details insignificant here.

Kuz'mina et al.[52] used the PMC program for the prediction of density of organic compounds with a high content of nitrogen. The same work was also made for a number of hypothetical nitramino caged compounds whose molecular structures had been predicted by theoretical computational methods.[50]

For the metastable polymorph of piracetam, a popular therapeutic agent, whose crystal structure was unknown except for the monoclinic cell dimensions, Dzyabchenko and Agafonov[49] found by energy minimization with PMC a number of possible structures with reasonable hydrogen-bond geometry. These structures were used as trial ones in the subsequent X-ray powder diffraction study,[53] which confirmed one of them to be true. The latter then was successfully refined by the Rietveld procedure to give the final structure with a low *R*-factor and reasonable crystal and molecular geometry.

The program is available free for academic use upon request to the first author. The standard package (up to 600 atoms in the asymmetric part) involves two executable modules running on a PC platform under MS DOS (DOS under Microsoft Windows), the test examples, and the instruction for users. The first module (pmcdat.exe) serves for the preparation of formatted input data to the second module (pmc.exe), which performs energy calculations. Both RAM and hard-drive space requirements are minimal (450 Kb and 5 Mb, respectively). The program input allows reading both free-format instruction and formatted coordinate entries retrieved from the Cambridge crystal structural database.

6. Solvated Dimer and Potassium-Doped Dimer

Prior to search for the unknown crystal structures of pressure-induced dimer, we performed calculations for the experimentally observed crystal structures: of the solvated C_{60} form containing four *o*-dichlorobenzene (DCB) molecules per one C_{60}[18] and of the dimeric alkali fulleride $K_2(C_{60})_2$.[19] In each case, the interaction potential for the guest component was not precisely known, and we used a few trial parametrizations based on the usual LJ plus electrostatic scheme, attempting to reach the closest agreement of the optimized crystal geometry with experiment. Throughout these calculations, the interaction potential for C_{60} dimers (section 4) remained fixed.

Solvated Dimer. The crystal disorder of the four DCB molecules in the observed structure presents an obvious problem, for the published coordinates[18] give rise to abnormally short intermolecular contacts C···Cl, C···C, and C···H (up to 2.2, 1.8, and 1.2 Å, respectively). Such contacts can be explained as resulting from statistical averaging of the various ordered solvent configurations which coexist in the matrix of $(C_{60})_2$ molecules. With this idea in mind, we carried out a search for such ordered solvent structures. The starting parameters were set at the experimental values for the six triclinic lattice dimensions and the three Euler angles of the $(C_{60})_2$ molecule in centrosymmetric position. The starting orientations for each solvent molecule were selected in turn from the two alternative orientations determined by experimental atomic coordinates with partial occupancy, this gave a total of eight starting solvent configurations. On arrival at the end minimization point, the changes in orientation of the solvent molecules were in all cases significant. On the contrary, the changes in the dimer molecule orientation were relatively small and concerned mostly the ψ angle rotation about the dimer axis. The relative stability of the energy minima corresponding to various solvent configurations was found sensitive to minor changes in the parametrization scheme for chlorine atoms and the atomic charges of the DCB molecule. The minimized structure showing reasonably good fit to the observed structure in the lattice dimensions and dimer molecule orientation at some choice of the potential parameters for the solvent molecules is given in Table 3. (The structural and the potential-field parameters of the solvent molecules are not presented there, but they are available from the first author of this paper on request.) With this result, we thus confirmed the interaction potential for C_{60} dimers to be good, in spite of evident problems caused by the crystal disorder of the solvent molecules.

Removing the four solvent molecules and subsequent relaxation of the remaining structure to the nearest energy minimum result in a triclinic pure dimer structure of $P\bar{1}$ symmetry (I in Table 5). Its cell dimensions and C_{60} positions conform to a distorted hcp lattice (space group $P6_3/mmc$) rather than fcc characteristic of the pressure-induced dimers to be considered below.

K-Doped Dimeric Fulleride. The single-bonded trans dimer is a molecule formally bearing the charge of two extra electrons.[19] We assumed this charge distributed uniformly over the 120 carbon atoms. The LJ parameters for K···C interaction were initially taken of 3.46 Å and −0.47 kcal/mol for ρ and ϵ, respectively.[57] However, the optimized structure revealed too large off-center displacements of the K atoms as compared to the observed structure.[19] Consequently, we tried various LJ parameter values that would give better agreement with experi-

TABLE 3: Comparison of the Observed and Predicted Structures of the Solvated and the Potassium-Doped Dimers

			K-doped trans dimer		
	solvated dimer				K-doped D_{2h} dimer
structure	obsd[a]	predicted	obsd[b,c]	predicted[d]	predicted[e]
space group	$P\bar{1}$	$P\bar{1}$	$P2_1/a$	$P2_1/a$	$P2_1/a$
E_{tot} (kcal/mol)		−155.86		−292.04	−336.24
E_{Coul} (kcal/mol)		−9.73		−176.48	−178.53
density (g/cm^3)	1.739	1.794	1.864	1.916	1.958
lattice constants (Å, deg)					
a	11.14	11.29	17.153	16.91	16.83
b	17.94	17.53	9.793	9.82	9.81
c	10.10	9.84	19.224	19.21	18.91
α	97.2	96.9	90.0	90.00	90.0
β	103.3	103.2	124.1	123.4	124.4
γ	94.4	92.5	90.0	90.0	90.0
C_{60} center coordinates					
x_o	0.021	0.061	0.007	0.010	0.008
y_o	0.226	0.230	0.000	−0.001	−0.001
z_o	−0.155	−0.153	0.246	0.247	0.245
Euler angles (deg)					
φ	62.0	61.7	−8.8	−9.2	0.1
θ	2.6	−4.7	−5.3	−4.3	1.5
ψ	9.2	−5.7	41.8	39.8	41.8

[a] Reference 18. [b] Reference 19. [c] K atoms at 0.0, 0.5, 0.013 and 0.0, 0.5, 0.513. [d] K atoms at 0.0, 0.5, 0.0 and 0.0, 0.518, 0.513. [e] K atoms at 0.0, 0.5, 0.0 and −0.002, 0.5, 0.525.

TABLE 4: Characteristics of the Dimer Lattices Derived from the FCC Lattice

lattice[a]	n_{dir}[b]	Z	unit cell[c]	possible space groups[d]
a	1	1	**a**, (**b** − **c**)/2, (**b** + **c**)/2	$P\bar{1}$
b	1	2	**a**, **b**, **c**	$P2_1/c$ ($A2/m$)
c	1	2	**a** − **c**, **b**, (**a** + **c**)/2	$P\bar{1}$, $P2_1$, $P112_1$ ($P2_12_12$), $Pn11$ ($P2/n11$, $Pmmn$)
d	1	1	(**a** + **b**)/2, (**b** + **c**)/2, −**a** + **c**	$P\bar{1}$
e	1	2	−(**a** − **c**)/2 + **b**, (**a** + **c**)/2, **a** − **c**	$P2_1/a$, ($C2/m$)
f	1	4	**a**, 2**b**, **c**	$I\bar{1}$
g	2	2	**a**, **b**, **c**	$P2_1/n$, ($P4_2/mcm$)
h	2	2	**a**, **b**, **c**	$P2/b11$, ($P4_2/mcm$)
i	2	4	**a**, **b**, 2**c**	$Pcab$ ($Ccmb$), $Pnaa$, $C2/n11$
j	1	2	(**a** − **c**)/2, (**a** + **c**)/2, 2**b**	$P2_1/c$
k	1	2	(**a** − **c**)/2, (**a** + **c**)/2, 2**b**	$P112_1/n$
l	2	2	**a** − **c**, (**a** + **c**)/2, **b**	$P112_1/c$
m	2	8	**a** − **c**, **a** + **c**, 2**b**	$A2/a$
n	4	8	**a** − **c**, **a** + **c**, 2**b**	$Pcab$
o	4	4	**a**, **b**, 2**c**	$P4_1$
p	3	3	$\mathbf{a}_h$, $\mathbf{b}_h$, 2$\mathbf{c}_h$	$P3_1$

[a] See Figure 2. [b] Number of unique directions of the dimer molecular axis. [c] **a**, **b**, and **c** are the cubic cell vectors of the parent C_{60} fcc lattice; $\mathbf{a}_h$ = (**a** − **c**)/2, $\mathbf{b}_h$ = (**a** + **c**)/2, and $\mathbf{c}_h$ = **a** + **b** + **c** are hexagonal axes of the fcc lattice. [d] Space groups are given assuming D_{2h} symmetry for the dimer with arbitrary ψ rotation except for those listed in parentheses, which are valid for particular ψ.

ment. We found the K off-center displacements very sensitive to the ρ change. On the contrary, changing ϵ had no marked influence on these characteristics and it was set on its initial value of −0.47 kcal/mol. The best ρ was found to be 3.65 Å; the corresponding optimization results are given in Table 3 in comparison with the experimental structure. Note that the off-center K atom displacements persisted until ρ was increased to 3.8 Å. The latter value is much greater than the critical parameter ρ_O value of 3.51 Å suggested by Goze et al.[57] for the octahedral site in C_{60}.

The last column in Table 3 presents a hypothetical structure of the D_{2h} dimer doped with two K, which was obtained by replacement in the observed structure of the single-bonded dimer molecule by the D_{2h} molecule, followed by the energy minimization. One can see that the two dimers are rather similar to each other in both the lattice dimensions and C_{60} positional and orientational parameters. When both K atoms were removed from the hypothetical dimeric fulleride, the structure came to one of the lowest-energy structures (III), to be discussed in subsequent section.

7. Predicted Structures of the Pressure-Induced $(C_{60})_2$

The structure prediction for such molecule as $(C_{60})_2$, comprising as many as 300 Lennard-Jones and electrostatic interaction centers, would present a computationally very expensive task if the search was made by scanning over the entire configuration space. Fortunately, as was stated above, with the pressure-induced dimer, the search is confined to the essentially fcc-like C_{60} lattices. To obtain starting dimer structures conforming to the fcc geometry, we derived, as a first step, the ideal dimer lattices composed of the fcc points connected in pairs along cubic face diagonals. Of the various such dimer lattices, we selected for calculations the sixteen shown in Figure 2. Their space-group symmetries and the unit-cell axes expressed in terms of the fcc lattice axes are listed in Table 4. Note that these lattices do not cover all the possible dimer configurations (whose number is in principle infinite, if one implies an aperiodic case). We believe, however, that the selected list is complete enough with respect to the variety of the *nearest-neighbor* molecular environments that are possible in the dimeric structures. Assuming the large size of the $(C_{60})_2$ molecules, one can find that the nearest-neighbor interactions represent the lattice energy almost totally, while the remote interactions give only a small fraction of it, in which the long-range electrostatic forces predominate.

Each dimer lattice was used to generate the corresponding set of initial structures of $(C_{60})_2$ molecules, where all parameters except ψ were defined by the particular dimer lattice. The ψ angles were changed in steps of 20° in the range 0−90° for all lattices except the triclinic ones; in the latter case the upper ψ limit was 180°.

As a result of the energy minimization of the initial structures, we found a variety of minima ranging in energy within a few kilocalories per mole and exhibiting various space-group symmetries. Numerical characteristics of the 10 most stable of them (II−XI) are given in Table 5. As expected, despite the various crystal classes to which the optimized structures exactly belong, their lattice geometries are approximately fcc. Neither of them is lower in energy than the hcp type structure I (section 6). The fact that the most stable lattice is not observed in the experimental spectra can be related to the high potential barrier separating the packings of both types. Thus, our calculation of the optimal transition path from I to IV, closest to I, in the space of triclinic structures, gave an estimate of the potential barrier from fcc to hcp C_{60} packing of about 10 kcal/mol.

The predicted structures show a range of densities which in the structure row II−XI do not necessarily correlate with the lattice energy. Thus, the most stable *Pbca* structure (II) is of a very low density while the least-stable *Cmca* structure (XI) presents the highest density. Under pressure, the relative stability of the 10 structures is changed. Table 6, where the optimized enthalpy ($H = E + pV$) values are compared for a number of competitive minima in a pressure range of up to 30 kbar, confirms this conclusion. Indeed, the *Pbca* structure, which is at normal pressure well below in energy than any other structure, loses its preference at even a few kilobar pressure. On the other hand, the densest *Cmca* structure becomes the most stable above

TABLE 5: Predicted Structures of the Pressure-Induced Dimer

	structure										
	I	II	III	IV	V	VI	VII	VIII	IX	X	XI
space group	$P\bar{1}$	*Pbca*	$P2_1/a$	$P\bar{1}$	$P2_1/c$	$P3_1$	$P\bar{1}$	$P3_1$	$P2_1/n$	$P2_1/c$	*Cmca*
E_{tot} (kcal/mol)	−79.25	−78.49	−77.96	−77.78	−77.47	−77.22	−77.13	−77.10	−77.00	−76.93	−76.52
E_{Coul} (kcal/mol)	−3.95	−6.21	−1.50	−2.60	−2.30	−3.95	−3.54	−3.82	−1.65	−4.74	0.54
density (g/cm^3)	1.832	1.817	1.836	1.829	1.832	1.816	1.817	1.817	1.832	1.810	1.838
lattice constants (Å, deg)											
a	9.92	13.97	17.04	9.93	9.73	9.84	9.93	9.85	13.56	13.86	13.62
b	9.69	13.71	9.67	9.73	13.55	9.84	9.88	9.85	13.65	13.86	13.87
c	15.76	27.52	19.04	19.78	19.84	47.13	19.77	47.03	14.12	13.78	27.58
α	92.6	90.0	90.0	59.4	90.0	90.0	58.6	90.0	89.0	90.0	90.0
β	87.2	90.0	123.8	57.5	92.62	90.0	57.5	90.0	90.0	93.2	90.0
γ	120.3	90.0	90.0	59.1	90.0	120.0	58.6	120.0	90.0	90.0	90.0
C_{60} center coordinates											
x_o	−0.150	0.001	0.009	0.033	−0.236	0.629	−0.036	0.637	0.236	0.244	0
y_o	0.162	−0.223	−0.001	−0.007	0.236	−0.005	−0.015	0.024	−0.237	0.0	−0.218
z_o	0.244	0.122	0.243	0.243	−0.120	0.081	0.244	0.081	0.0	0.234	0.123
Euler angles (deg)											
φ	−20.1	42.4	0.1	1.5	54.6	−18.1	3.0	−19.3	90.9	0.0	41.6
θ	−30.0	0.2	1.7	−59.8	30.4	27.2	−59.8	27.2	44.7	48.1	0.0
ψ	20.7	43.6	62.6	23.8	85.4	17.7	−18.1	−18.9	30.1	42.2	90.0

20 kbar. Within the 0−30 kbar range, a total of six dimer structures are in competition with each other.

From a comparison of densities in parallel with Coulomb energies, E_{Coul}, in the structure row of Table 5, one can see that large E_{Coul} correspond, as a rule, to low-density structures, while small E_{Coul} occur with structures of high density. We explain this by the tendency of the electrostatic forces in $(C_{60})_2$ to orient the molecules in a way that does not let them fill the space less quite effectively. Obviously, filling the space effectively requires intermolecular interaction of unoriented nature such as of van der Waals type. Pressure due to the *pV* term in the expression for enthalpy signifies the van der Waals component in the total energetic balance and, correspondingly, weakens the electrostatic one. This is best illustrated by both above examples: the *Pbca* structure, with E_{Coul} most negative, and the *Cmca* structure, where E_{Coul} is even a bit positive.

Previous examples of such a competition of the electrostatic and van der Waals forces involve the P/H transition in the sc C_{60} phase in the low-pressure region, and its further change into the densest *Cmca* structure predicted at 40 kbar.[33]

8. Structural Similarities and Phase Connections

The position and orientation of the eight C_{60} cages in the unit cell of the *Pbca* structure (II in Table 5) can be described as composed of two blocks of four C_{60} units of approximately cubic shape. Moreover, each block in itself is similar to the unit cell of the monomeric *Pa*3-P structure with respect to both its overall dimensions and the position and orientation of the four C_{60}. Thus, the set of Euler angles for C_{60} in Table 5 for structure II can be brought through a rotation about one of the 5-fold symmetry axes of the buckyball, to an equivalent set $\varphi = -15.5°$, $\theta = -19.3°$, $\psi = -9.0°$, whose deviation from the respective three angles in *Pa*3-P in Table 1 can be also characterized by an overall turn angle $\omega = 10°$, which is small enough. The principal difference of the two structures, however, is that the adjacent blocks contact along [001] through the centrosymmetry operation in the dimer structure while through *c*-axis translation in the monomer. It is interesting that the analogy of the *Pbca* dimer with the sc-P monomer is also present in their pressure behavior, for both are the most stable structures at normal pressure and both lose energetic preference at a low pressure (Table 6).

In the monoclinic $P2_1/a$ structure (III), the dimer molecules are packed head to tail along **c**. The C_{60} positional and orientational parameters as well as the six lattice dimensions are similar to those of the monomeric *Cmca* structure in Table 1 (one can see this after applying the cell transformation $\mathbf{a}' = \mathbf{b} + \mathbf{c}/2$, $\mathbf{b}' = (\mathbf{a} + \mathbf{b})/2$, $\mathbf{c}' = -(\mathbf{a} - \mathbf{b} + \mathbf{c})/2$ to the $P2_1/a$ structure parameters in Table 6, giving rise to $a' = 13.57$, $b' = 9.80$, $c' = 9.81$ Å and $\alpha = 92.4$, $\beta = 89.4$, $\gamma = 89.3°$), with the deviation parameter $\omega = 15°$ between the respective C_{60} orientations.

At the same time, III is similar to the *Pnnm* structure of the polymeric O phase, with a small angular deviation of $\omega = 3°$. The rotation of the dimer molecule from the optimal $P2_1/a$ configuration to the more symmetrical *Pnnm* configuration, with the dimer molecule aligned exactly the same way as the linear chain in the polymeric structure, results in the loss of potential energy of about 0.1 kcal/mol.

For the monoclinic $P2_1/n$ structure (IX), we can point out its relationship with a perfectly tetragonal (space group $P4_2/mmc$) structure. The latter, however, does not occur as one of the low-energy minima but corresponds to a shallow crater on the top of a mountain 4.5 kcal/mol higher in energy than IX. This mountain separates the energy minimum IX at $\psi = 30°$, $\beta = 89°$ from the symmetry-equivalent one (IX′) at $\psi = -30°$, $\beta = 91°$. The $P4_2/mmc$ dimer ($a = b = 13.99$, $c = 13.45$ Å; $\varphi = 90$, $\theta = 45$, $\varphi = 0°$) is similar to the tetragonal-layer polymer structure of the same symmetry (Table 2), whose parameters after the cell transformation $\mathbf{a}' = (\mathbf{a} - \mathbf{b})/2$, $\mathbf{b}' = (\mathbf{a} + \mathbf{b})/2$, $\mathbf{c}' = \mathbf{c}$ are $a' = b' = 12.85$, $c' = 14.75$ Å and $\varphi = 90$, $\theta = 45$, $\psi = 0°$.

The triclinic dimer structures IV and VII show similarity with respect to each other and the rhombohedral polymer $R\bar{3}m$-II (Table 2). The C_{60} orientation in VII deviates by $\omega = 18°$ from that in the $R\bar{3}m$-II polymer and by $\omega = 15°$ from the hypothetical monomer $R\bar{3}$ (Table 1). The corresponding deviations for IV are $\omega = 25$ and 21°. With the pressure increased, these deviations tend to increase for V, while decreasing for VII. The optimal path from V to VII passes through an almost perfectly $R\bar{3}m$ symmetrical configuration at the top of a potential barrier of 22 kcal/mol as high, whose parameters are close to that of the $R\bar{3}m$-II polymer.

The found similarities between the monomeric, dimeric, and polymeric C_{60} structures make it worth a suggestion that the respective structures are connected states in the conversions path from the fcc C_{60} to its pressure-induced polymeric products. The most remarkable path involves the conversion of the $P2_1/a$

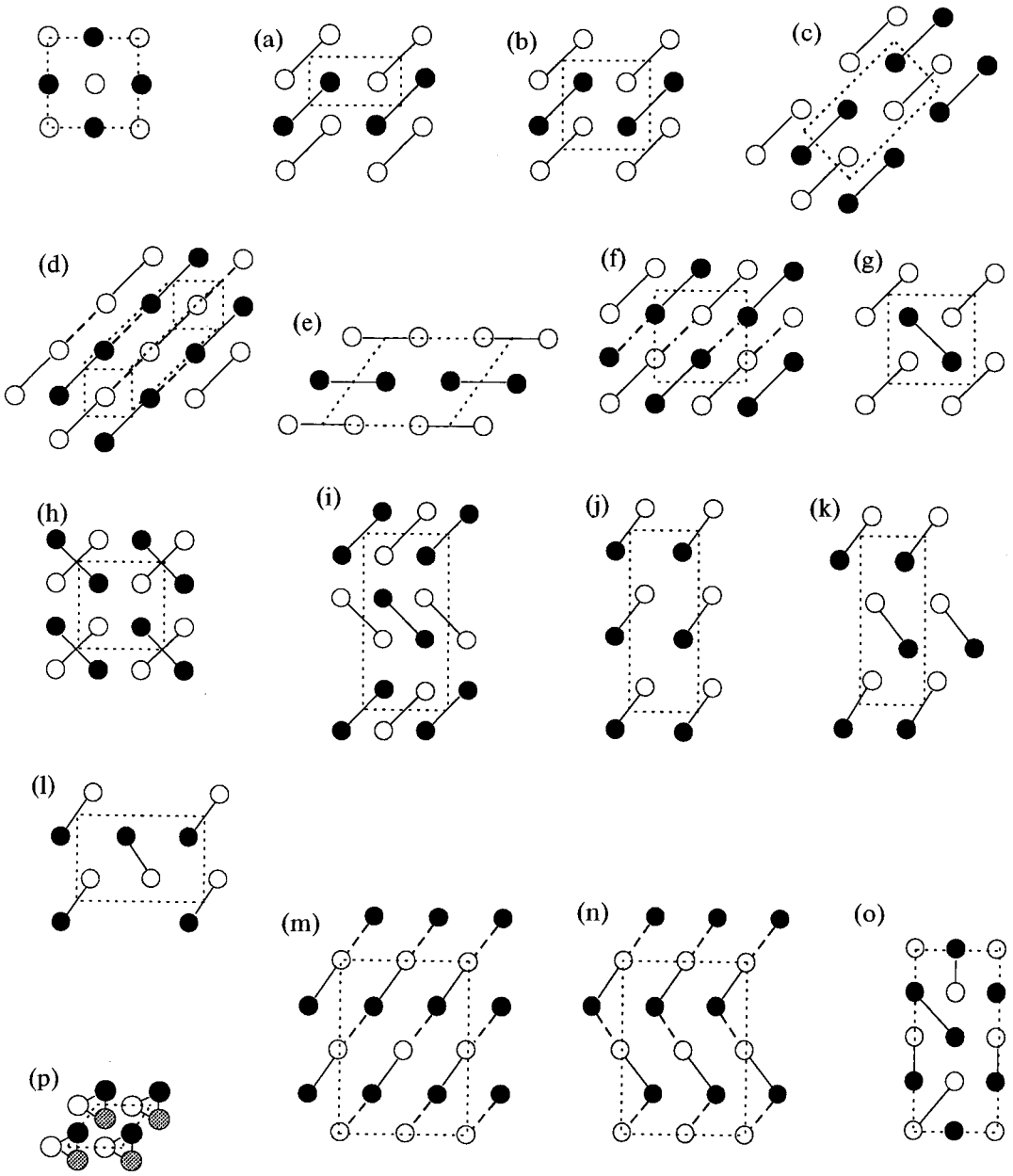

Figure 2. Schematic drawings of the dimer lattices derived from the fcc lattice (see Table 4 for the unit-cell axes and space groups). Except in (p), empty and dark circles designate lattice points at $y = 0$ and $^1/_2$ of an fcc lattice translation $\mathbf{b}'$ normal to the paper sheet plane, $\mathbf{b}' = \mathbf{b}$ for (a)−(d), (g)−(i), and (o) and $\mathbf{b}' = (\mathbf{a} + \mathbf{c})/2$ for (e) and (j)−(n). Dashed lines show dimers at $y = 1$ and $-^1/_2$ (whenever they do not coincide with those at 0 and $^1/_2$, respectively). For (p): empty, shadow, and dark circles stand for $z = 0$, $^1/_3$, and $^2/_3$ of the $\mathbf{c}_h$ translation, respectively.

TABLE 6: Enthalpies (kcal/mol) of the Dimer Structures at Different Pressures

pressure (kbar)	structure					
	II	III	IV	V	IX	XI
0	−78.5	−78.0	−77.7	−77.5	−77.0	−76.5
5	13.9	13.5	14.0	14.3	14.5	14.7
10	106.3	104.9	105.4	105.6	105.9	105.7
15	197.5	195.3	195.6	195.8	196.2	195.5
20	287.8	284.9	284.9	285.1	285.7	284.4
25	377.4	373.7	373.4	373.6	374.3	372.4
30	466.2	461.9	461.2	481.3	462.4	459.8

dimer into the *Pnnm* chain polymer, for the geometrical and the energetic changes are minimal here. The almost perfectly head-to-tail arrangement of the successive dimers along [001] is geometrically extremely favorable for the attachment of successive dimers to one another through [2+2] cycloaddition. Thus, there are structural reasons for the formation of higher than dimer linear-chain oligomeric C_{60} products isostructural to the $P2_1/a$ dimer, where the oligomer chain length is reflected in the average *c*-axis length per one C_{60}. The model does not exclude a continuous distribution of the oligomeric chains by their length. It would be interesting in further investigations to test the model experimentally, for instance, in application to the kinetics of C_{60} polymerization.

The paths from C_{60} dimer to the tetra- and hexagonal-layer polymers, according to this scheme, require a significant $\Delta\psi$ rotation of about 30° with a high loss in the packing energy (4.5 and 22 kcal/mol, respectively). These energetic expenses are affordable due to the negative energy of the forming interfullerene covalent bonds.

The dimer to polymer conversion paths are obviously in competition with the direct monomer to polymer paths. To investigate more precisely the role of the different solid states in C_{60} polymerization a theoretical model more sophisticated than we presently have is necessary. Such a theoretical model

must incorporate, in addition to the nonbonded interaction potential, a specific intermolecular interaction term that would be responsible for [2+2] chemical bonding. Our work in this direction is currently in progress.

9. Conclusion

We have presented a theoretical study of the dimeric solid formed under pressure from the fcc C_{60} through [2+2] cycloaddition of double bonds. Its key idea based on the X-ray diffraction evidence is that the solid-state dimerization does not change significantly the original fcc positions of C_{60} molecules. We applied a bond charge interaction potential model of Lu et al., proved successful in the previous work on the monomeric and polymeric C_{60} structures, to predict the structures of dimeric C_{60}. On inclusion of additional terms to account for the guest particles, the model was found to be good for the prediction of the experimentally known structures of the solvated dimer and the alkali-doped dimer. The predicted dimer structures show various space-group symmetries, but the constituting C_{60} retain an approximately fcc packing. Their relative stability is changed under pressure, being determined by the interplay of the Lennard-Jones and Coulomb forces. Some dimer structures are remarkably similar to the monomeric and polymeric C_{60} packings. On this basis we have proposed that the involved structures are possible connected states in the conversion paths from monomeric C_{60} to the pressure-polymerized states. One of the dimer structures is geometrically favorable for the formation of higher than dimer C_{60} chain oligomers as well as the infinite polymer. Overall, in this paper we have demonstrated the power of our theoretical approach, which is based on the use of structure-prediction and structure-comparison techniques. Such an approach is promising in studies of the structure-based properties of solid molecular materials, whose crystal structure is poorly resolved experimentally.

Acknowledgment. A.V.D. and V.A.D. acknowledge support from the Russian Foundation for Basic Research (grants 97-03-33584a and 99-03-32962a).

References and Notes

(1) Rao, A. M.; Zhou, P.; Wang, K. A.; Hager, G. T.; Holden, J. M.; Wang, Y.; Lee, W. T.; Bi, X.-X.; Eklund, P. C.; Cornett, D. S.; Duncan, M. A.; Amster, I. J. *Science* **1993**, *259*, 955.

(2) Iwasa, Y.; Arima, N.; Fleming, R. M.; Siegrist, T.; Zhou, O.; Haddon, R. C.; Rothberg, L. J.; Lyons, K. B.; Carter, H. L., Jr.; Hebard, A. F.; Tycko, R.; Dabbagh, G.; Krajewski, J. J.; Thomas, G. A.; Yagi, T. *Science* **1994**, *264*, 1570.

(3) Núnez-Regueiro, M.; Marques, L.; Hodeau, J.-L.; Béthoux, O.; Perroux, M. *Phys. Rev. Lett.* **1995**, *74*, 278.

(4) Xu, C. H.; Scuseria, G. E. *Phys. Rev. Lett.* **1995**, *74*, 274.

(5) Rao, A. M.; Eklund, P. C.; Hodeau, J.-L.; Marques, L.; Núnez-Regueiro, M. *Phys. Rev. B* **1997**, *55*, 4766.

(6) Agafonov, V.; Davydov, V. A.; Kashevarova, L. S.; Rakhmanina, A. V.; Kahn-Harari, A.; Dubois, P.; Céolin, R.; Szwarc, H. *Chem. Phys. Lett.* **1997**, *267*, 193.

(7) Moret, R.; Launois, P.; Persson, P.-A.; Sundqvist, B. *Europhys. Lett*. **1997**, *40*, 55.

(8) Davydov, V. A.; Kashevarova, L. S.; Rakhmanina, A. V.; Dzyabchenko, A. V.; Agafonov, V.; Dubois, P.; Céolin, R.; Szwarc, H. *JETP Lett*. **1997**, *66*, No. 2, 120.

(9) Davydov, V. A.; Kashevarova, L. S.; Rakhmanina, A. V.; Agafonov, V.; Allouchi, H.; Céolin, R.; Dzyabchenko, A. V.; Senyavin, V. M.; Szwarc, H. *Phys. Rev. B* 1**998**, *58*, 14786.

(10) Sundqvist, B. Fullerenes Under High Pressures. Department of Experimental Physics, Umea University: Umea, Sweden, 1998. (To be published in *Adv. Phys.*).

(11) Burger, B.; Winter, J.; Kuzmany, H. *Z. Phys. B* **1996**, *101*, 227.

(12) Persson, P.-A.; Edlund, U.; Jacobsson, P.; Johnels, D.; Soldatov, A.; Sundqvist, B. *Chem. Phys. Lett.* **1996**, *258*, 540.

(13) Davydov, V. A.; Kashevarova, L. S.; Rakhmanina, A. V.; Agafonov, V.; Céolin, R.; Szwarc, H. *Carbon* **1997**, *35*, 735.

(14) Adams, G. B.; Page, J. B.; Sankey, O. F.; O'Keefe, M. *Phys. Rev. B* **1994**, *50*, 17471.

(15) Menon, M.; Subbaswamy, K. R.; Sawtarie, M. *Phys. Rev. B* **1994**, *49*, 13966.

(16) Porezag, D.; Pederson, M. R.; Frauenheim, Th.; Kohler, Th. *Phys. Rev. B* **1995**, *52*, 14963.

(17) Porezag, D.; Jungnickel, G.; Frauenheim, Th.; Seifert, G.; Ayuela, A.; Pederson, M. R. *Appl. Phys.* **1997**, *A64*, 321.

(18) Wang, G.-W.; Komatsu, K.; Murata, Y.; Shiro, M. *Nature* **1997**, *387*, 583.

(19) Oszlányi, G.; Bortel, G.; Faigel, G.; Granasy, L.; Bendele, G. M.; Stephens, P. W.; Forro, L. *Nature* **1996**, *54*, 11849.

(20) Komatsu, K.; Wang, G.-W.; Murata, Y.; Shiro, M. In *Recent Advances in the Chemistry and Physics of Fullerenes and Related Materials*; Kadish, K. M., Ruoff, R. S., Eds.; Electrochemical Society: Pennington, NJ, 1997; Vol. 4, p 291.

(21) Lebedkin, S.; Gromov, A.; Giesa, S.; Gleiter, R.; Renker, B.; Rietschel, H.; Kratschmer, W. *Chem. Phys. Lett.* **1998**, *285*, 210.

(22) Davydov, V. A.; Kashevarova, L. S.; Rakhmanina, A. V.; Agafonov, V.; Allouchi, H.; Céolin, R.; Dzyabchenko, A. V.; Senyavin, V. M.; Szwarc, H.; Tanaka, T.; Komatsu, K. *J. Phys. Chem. B* in press.

(23) Guo, Y.; Karasawa, N.; Goddard, W. A., III; *Nature* **1991**, *351*, 464.

(24) David, W. I. F.; Ibberson, R. M.; Dennis, T. J. S.; Hare, J. P.; Prassides, K. *Europhys. Lett*. **1992**, *18*, 219.

(25) Lu, J. P.; Li, X.-P.; Martin, R. M. *Phys. Rev. Lett*. **1992**, *68*, 1551;

(26) Sprik, M.; Cheng, A.; Klein, M. L. *J. Phys. Chem.* **1992**, *96*, 2027.

(27) Burgos, E.; Halac, E.; Bonadeo, H. *Phys. Rev. B* **1993**, *47*, 13903; **1994**, *49*, 15544.

(28) Pintschovius, L.; Chaplot, S. L. *Z. Phys.* **1995**, *B98*, 527.

(29) Dzyabchenko, A. V.; D'yachkov, P. N.; Agafonov, V. N. *Russ. Chem. Bull*. **1995**, *44*, 1408.

(30) Dzyabchenko, A. V.; Shilnikov, V. I.; Suslov, I. A. *J. Struct. Chem.* **1997**, *38*, 936.

(31) Dzyabchenko, A. V. To be published.

(32) Dzyabchenko, A. V.; Agafonov, V. N. *Russ. J. Phys. Chem*. **1998**, *72*, 1702.

(33) Dzyabchenko, A. V.; Agafonov, V. N. *Russ. J. Phys. Chem*. **1998**, *72*, 1822.

(34) Lundin, A.; Sundqvist, B. *Phys. Rev. B* **1996**, *53*, 8329.

(35) Agafonov, V.; Davydov, V. A.; Dzyabchenko, A. V.; Céolin, R.; Szwarc, H. In *Fullerenes. Recent Advances in the Chemistry and Physics of Fullerenes and Related Materials*; Kadish, K. M., Ruoff, R. S., Eds.; The Electrochemical Society: Pennigton, NJ, 1997; Vol. 5, p 373.

(36) Davydov, V. A.; Agafonov, V.; Dzyabchenko, A. V.; Céolin, R.; Szwarc, H. *J. Solid State Chem*. **1998**, *141*, 164.

(37) Dzyabchenko, A. V.; Agafonov. V.; Davydov, V. A. *Crystallogr. Rep*. **1999**, *44* (1) (Paper 1, in press).

(38) Dzyabchenko, A. V.; Agafonov, V.; Davydov, V. A. *Crystallogr. Rep.* **1999**, *44* (1) (Paper 2, in press).

(39) Basilevsky, M. V.; Weinberg, N. N.; Zhulin, V. M. *J. Chem. Soc., Faraday Trans. 1* **1985**, *81*, 875.

(40) Dzyabchenko, A. V. *Acta Crystallogr*. **1994**, *B50*, 414.

(41) Dzyabchenko, A. V. *Crystallogr. Rep*. **1997**, *42*, 207.

(42) Dzyabchenko, A. V.; Belskii, V. K.; Zorkii, P. M. *Sov. Phys. Crystallogr*. **1979**, *24*, 127.

(43) Dzyabchenko, A. V. *Sov. Phys. Crystallogr*. **1983**, *28*, 466.

(44) Williams, D. E. *Acta Crystallogr*. **1971**, *A27*, 452.

(45) Fletcher, R. Fortran Subroutines for Minimization by quasi-Newton. AERE-R7125, 1972.

(46) Gibson, K. D.; Scheraga, H. A. *J. Phys. Chem.* **1995**, *99*, 3752.

(47) Dzyabchenko, A. V. *Acta Crystallogr*. **1983**, *A39*, 941.

(48) (a) Dzyabchenko, A. V. *J. Struct. Chem.* **1984**, *25*, 416. (b) Dzyabchenko, A. V. *Ibid*., p 559. (c) Dzyabchenko, A. V.; Bazilevskii, M. V. *J. Struct. Chem*. **1985**, *26*, 553. (d) Dzyabchenko, A. V.; Bazilevskii, M. V. *Ibid*., p 558. (e) Dzyabchenko, A. V. *J. Struct. Chem*. **1986**, *27*, 412. (f) Dzyabchenko, A. V. *J. Struct. Chem*. **1987**, *28*, 862. (g) Dzyabchenko, A. V. *Sov. Phys. Crystallogr*. **1989**, *34*, 131.

(49) Dzyabchenko, A. V.; Agafonov V. N. *Proceedings of the 28th Hawaii International Conference on System Sciences (Jan. 3−6, 1995)*; Hunter, L., Shriver, B., Eds.; IEEE Computer Press: Los Alamitos, CA, 1995; Vol. 5 (Biotechnology Computing), p 237.

(50) Dzyabchenko, A. V.; Pivina, T. S.; Arnautova, E. A. *J. Mol. Struct*. **1996**, *378*, 67.

(51) Belsky, V. K.; Zorkii, P. M. *Acta Crystallogr*. **1977**, *A33*, 1004.

(52) Kuz'mina, N. E.; Pirogova, N. A.; Pivina, T. S.; Schlyapochnikov, V. A. *Zh. Fiz. Khimii* **1992**, *66*, 101 (in Russian).

(53) Louer, D.; Louer, M.; Dzyabchenko, A. V.; Agafonov, V.; Céolin, R. *Acta Crystallogr*. **1995**, *B51*, 182.

(54) Gibson, K. D.; Scheraga, H. A. *J. Phys. Chem.* **1995**, *99*, 3765.

(55) Thiéry, M. M.; Rérat, C. *J. Chem. Phys.* **1996**, *104*, 9079.

(56) van Eijck, B. P.; Spek, A. L.; Mooji, W. T. M.; Kroon, J. *Acta Crystallogr*. **1998**, *B54*, 291.

(57) Goze, T.; Apostol, M.; Rachdi, F.; Mehring, M. *Phys. Rev. B* 1**995**. *52*, 15031.